Atomic and electronic structure of MoS2 nanoparticles

Bollinger, Mikkel; Jacobsen, Karsten Wedel; Nørskov, Jens Kehlet

Link back to DTU Orbit

Atomic and electronic structure of MoS$_2$ nanoparticles

M. V. Bollinger, K. W. Jacobsen, and J. K. Nørskov

Center for Atomic-scale Materials Physics, Department of Physics, Technical University of Denmark,
DK−2800 Kongens Lyngby, Denmark

Using density-functional theory (DFT) we present a detailed theoretical study of MoS$_2$ nanoparticles. We focus on the edge structures, and a number of different edge terminations are investigated. Several, but not all, of these configurations have one-dimensional metallic states localized at the edges. The electronic structure of the edge states is studied and we discuss their influence on the chemical properties of the edges. In particular, we study the reactivity towards hydrogen and show that hydrogen may form stable chemical bonds with both the two low-Miller indexed edges of MoS$_2$. A model for calculating Gibbs free energy of the edges in terms of the DFT energies is also presented. This model allows us to determine the stable edge structure in thermodynamic equilibrium under different conditions. We find that both the insulating and metallic edges may be stable depending on the temperature and the composition of the gas phase. Using the Tersoff-Hamann formalism, scanning-tunneling microscopy (STM) images of the edges are simulated for direct comparison with recent STM experiments. In this way we identify the experimentally observed edge structure.

I. INTRODUCTION

MoS$_2$ is a remarkable material in the sense that it has a number of interesting, yet very different, properties. Here we name four: (i) the ability to form nanotubes. MoS$_2$ is a layered material and experimentally it has been demonstrated that a single layer of MoS$_2$, like graphene, can be warped into nanotubes.[1] (ii) MoS$_2$ can work as a catalyst. MoS$_2$ particles form the basis for the catalyst used in the hydrodesulferization (HDS) process.[2] This is one of the first steps in oil refining where sulfur is removed from the crude oil. It is generally believed that the active sites are located at the edges of the catalyst particles and are associated with the presence of coordinatively unsaturated Mo atoms. (iii) MoS$_2$ is an effective solid lubricant. MoS$_2$ fullerenelike particles have been reported to have very low friction and wear properties.[3,4] This makes MoS$_2$ an important material when liquid lubricants are impractical, such as in space technology and ultrahigh vacuum. (iv) MoS$_2$ can generate one-dimensional, conducting-electron states. Recently we reported that one-dimensional, metallic states are localized at the edges of MoS$_2$ nanoparticles.[5] Experimentally triangular shaped, single-layer MoS$_2$ nanoparticles can be grown on a reconstructed Au(111) surface[6] and studied using scanning-tunneling microscopy (STM).[7,8] In Ref. 5 we showed that a bright brim of high conductance extending along the edges of the MoS$_2$ nanoclusters is associated with such a metallic edge state.

In this paper we present a detailed theoretical study of single-layer MoS$_2$ nanostructures. The focus is on the edges of the nanoparticles, and their structural and electronic properties are analyzed using density-functional theory (DFT). In particular, we shall investigate the two low-Miller index edges: the so-called Mo edge and S edge. We show that one-dimensional edge states are localized at both types of edges but we also find that their electronic structure is crucially dependent on the edge termination. For instance, the different structures may be either metallic or insulating. The electronic structure ultimately also determines the chemical properties. Using hydrogen as a probe we investigate the chemical activity of the edges and find that hydrogen may adsorb at both the Mo edge and the S edge.

Based on the DFT results we construct a thermodynamic model for the MoS$_2$ edges allowing us to investigate their atomic structure under various conditions. It is shown that both the metallic and insulating edges may be stable depending on the ambient pressure and temperature. Moreover, in a hydrogen-rich environment, e.g., HDS conditions, we find that atomic hydrogen will be adsorbed at both the Mo edge and the S edge. The abundance of hydrogen at the edges is important since during the catalytic reaction the sulfur-containing oil molecules are reduced by hydrogen.

Experimentally MoS$_2$ nanoparticles have recently been investigated using STM.[7] They were synthesized on a reconstructed Au(111) substrate and were reported to have a triangular morphology. Based on the DFT calculations we simulate STM images of the MoS$_2$ edges and these images are then used to identify the experimentally observed edge structure. The STM experiment is also discussed in terms of the thermodynamic model.

This paper is organized in the following way: in Sec. II the details of the DFT calculations are given and Sec. III describes the thermodynamic model for the MoS$_2$ edges. In Sec. IV the theoretical method used for simulating STM images is outlined. The atomic and electronic properties of bulk MoS$_2$ are presented in Sec. V and the STM imaging of the MoS$_2$ basal plane with and without an underlying Au substrate is discussed in the subsequent section. Section VII is devoted to an atomic and electronic structure analysis of the Mo edge. This includes a discussion of the influence of Au on the Mo edge. In Sec. VIII we investigate the possibilities for hydrogen adsorption at the Mo edge. Section IX is devoted to a study of the atomic and electronic structure at the S edge. Here we also investigate the possibilities for hydrogen adsorption at this edge termination. In Sec. X we discuss the effects caused by having finite-size MoS$_2$ edges. We
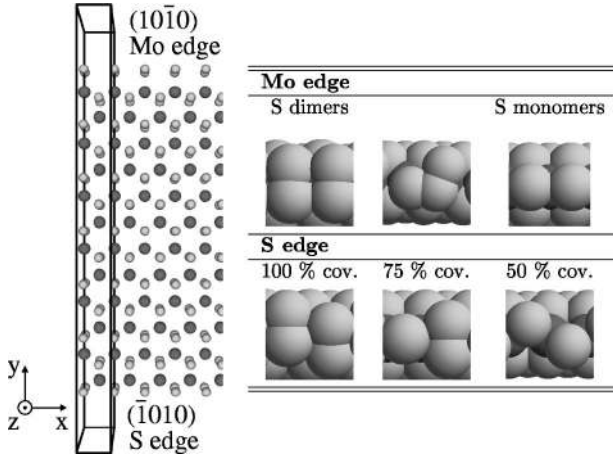
FIG. 1. Left: top view of the (0001) surface of a (1,12) single-layer MoS_2 stripe. The stripe is terminated by the $(10\bar{1}0)$ molybdenum edge (Mo edge) and the $(\bar{1}010)$ sulfur edge (S edge). The bright spheres represent S atoms whereas the dark spheres correspond to Mo atoms. The outline of the unit cell is indicated furthest to the left. Right: edge terminations of the Mo edge and S edge viewed from the sides of the edges. The MoS_2 stripe shown on the left is seen to have S dimers adsorbed at the Mo edge and a fully covered S edge.

compare the theoretical analysis with recent experimental STM data in Sec. XI and finally a summary is provided in Sec. XII.

II. SETUP AND CALCULATIONAL DETAILS

Bulk MoS_2 is a layered material and a single layer consists of an S-Mo-S sandwich. In each such layer the Mo atoms are arranged in a hexagonal lattice and are positioned in a trigonal prismatic coordination with respect to the two S layers. This implies that each Mo atom is coordinated by six S atoms. A single layer of MoS_2 can be terminated by two different low-Miller index edges: the sulfur-terminated $(\bar{1}010)$ edge and the molybdenum-terminated $(10\bar{1}0)$ edge. They will be referred to as the S edge and Mo edge, respectively. A number of different structures are feasible at each of these edges, see Fig. 1, but the more detailed description of their geometric structure is deferred to Secs. VII and IX.

The edges of single-layer MoS_2 are investigated in a model system consisting of a stripe of MoS_2 that is repeated in a supercell geometry, as illustrated in Fig. 1. Along $\langle 0001 \rangle$ there is 8.8 Å of vacuum between the repeated planes and they are separated by 8.9 Å of vacuum in the direction perpendicular to the edges. The upper and lower sides of the stripe are terminated by the Mo edge and S edge, respectively. In the following the size of a MoS_2 stripe will be indicated by the number of Mo atoms in the (x,y) directions, (n_x, n_y), contained within a single unit cell.

The density-functional calculations are carried out as follows:[9–12] The Kohn-Sham (KS) orbitals are expanded in plane waves with kinetic energies below 25 Ry.[13] The first Brillouin zone is sampled in a one-dimensional grid[14] with a separation of 0.16 Å^{-1} between neighboring $\boldsymbol{k}$ points. For a

supercell having a periodicity of one in the x direction, see Fig. 1, this corresponds to 12 $\boldsymbol{k}$ points. The ionic cores are replaced by ultrasoft pseudopotentials,[15] and in order to treat exchange and correlation effects the Perdew-Wang 1991 (PW91) functional is used.[16] First, the single-electron KS equation is solved by iterative diagonalization and the resulting KS eigenstates are populated according to the Fermi distribution. Then Pulay mixing of densities is applied, and the entire procedure is repeated until a self-consistent electron density is obtained. The total energies are subsequently extrapolated to zero temperature.[17] In all calculations the entire atomic structure is optimized by allowing the individual atoms to relax according to the calculated Hellmann-Feynman forces.

III. THERMODYNAMIC MODEL

In order to investigate the relative stability of the edge terminations under different thermodynamic conditions it is desirable to extend the DFT results to finite temperatures. In this section we shall derive an approximate scheme for calculating the Gibbs free energy of an MoS_2 edge in the presence of an atmosphere containing both H_2S and H_2. This model allows us to study the edges of MoS_2 in terms of a set of experimentally tunable parameters (T, p_{H_2S}, p_{H_2}), temperature and partial pressure of H_2S and H_2, respectively. The approach is based on a general methodology that has previously been applied in Refs. 18–20.

A. Edge free energy

We consider an MoS_2 stripe on the form shown in Fig. 1, and define its edge free energy γ as

$$\gamma = \frac{1}{2L}[G_{\text{stripe}}(MoS_2 + N_H H) - N_{Mo}\mu_{Mo} - N_S\mu_S - N_H\mu_H],$$
(1)

where $G_{\text{stripe}}(MoS_2 + N_H H)$ is the Gibbs free energy of a single unit cell. N_i and μ_i refer to the number of atoms in the unit cell and the chemical potential, respectively, of element i. L is the length of the edge. The most stable configuration will then be the one that minimizes γ. The factor of 2 in Eq. (1) indicates that the stripe exposes both the Mo edge and the S edge and hence γ represents the average edge free energy of the two edges. This means that we can study the relative stability of configurations located at the same edge provided that the configurations at the opposite edge are identical. On the other hand the edge free energy of the individual edges cannot be evaluated and hence the model does not give any information on the relative stability between the S edge and Mo edge. We also note that by retaining the chemical potential of hydrogen in the definition of γ, the possibility for hydrogen adsorption on the MoS_2 stripe is included in the model.

If the MoS_2 stripe is sufficiently large the edges will be in thermodynamic equilibrium with bulk MoS_2, i.e.,

$$g_{MoS_2}^{\text{bulk}} = \mu_{Mo} + 2\mu_S,$$
(2)

where $g_{MoS_2}^{bulk}$ is the Gibbs free energy of a formula unit of an infinite MoS$_2$ sheet. Hence the chemical potentials μ_S and μ_{Mo} cannot be varied independently and inserting this constraint in Eq. (1) yields

$$\gamma = \frac{1}{2L}[G_{stripe}(MoS_2 + N_H H) - N_{Mo} g_{MoS_2}^{bulk}$$

$$+ (2N_{Mo} - N_S)\mu_S - N_H \mu_H]. \tag{3}$$

We now proceed to express the free energies of the solid states entering Eq. (3) in terms of their corresponding DFT energies. In general the Gibbs free energy can be written in terms of the Helmholtz free energy f as $g = f + pV$, where p is the pressure and V is the volume. For solids the last term is negligibly small and can be omitted. For the temperatures in question, $T \ll T_F$, the electronic degrees of freedom will be almost completely frozen out and thus $f_{elec} \simeq E_{elec}$ is a good approximation. We can then write the free energy of the solid as[21]

$$g_{solid} \simeq E_{solid} + f_{vib}, \tag{4}$$

where the electrostatic energy of the ions is included in E_{solid} and f_{vib} is the Helmholtz free energy due to the lattice vibrations. We now make the approximation and assume $g_{solid} \simeq E_{solid}$, thus neglecting the vibrational contributions to the Helmholtz free energy. The edge free energy in turn becomes

$$\gamma = \frac{1}{2L}[E_{stripe}(MoS_2 + N_H H) - N_{Mo} E_{MoS_2}^{bulk}$$

$$+ (2N_{Mo} - N_S)\mu_S - N_H \mu_H]. \tag{5}$$

The validity of this expression relies on the importance of f_{vib}. Within the harmonic approximation for lattice vibrations this quantity is given by

$$f_{vib} = \sum_i \int \frac{d\mathbf{k}}{\Omega_{BZ}} \left\{ \frac{1}{2}\hbar\omega_i(\mathbf{k}) + k_B T \ln\left[1 - \exp\left(-\frac{\hbar\omega_i(\mathbf{k})}{k_B T}\right)\right]\right\}, \tag{6}$$

where Ω_{BZ} is the volume of the first Brillouin zone and the sum runs over all vibration modes. Since a large part of the MoS$_2$ stripe is bulklike we expect that the vibrational contributions from this region are canceled by the corresponding terms associated with $N_{Mo} g_{MoS_2}^{bulk}$, see Eq. (3). Hence the main approximation of Eq. (5) amounts to the omission of the lattice vibrations at the edges. The optical vibration frequencies of a sheet of MoS$_2$ have been measured at $\mathbf{k} = \Gamma$ to be around 400 cm^{-1} using Raman spectroscopy.[22] In order to obtain an estimate of the corresponding Helmholtz free energy we assume the modes to be dispersionless and find $f_{vib} \sim 10^{-2}$ eV per mode at room temperature. Hence, if the frequencies at the edges are not significantly changed the vibrational contribution will be small and thus Eq. (5) represents a reasonable approximation. If, on the other hand, the frequencies at the edges are significantly perturbed the validity of Eq. (5) will be more limited.

B. Chemical potentials

In this section we derive two expressions for the chemical potentials entering Eq. (5) that enable us to estimate these quantities in terms of the DFT energies for the isolated H$_2$ and H$_2$S molecules. We start by examining the chemical potential of an ideal gas, $\mu_{gas}(T,p)$. This quantity can be expressed in terms of a reference pressure, p^0:

$$\mu_{gas}(T,p) = \mu_{gas}(T,p^0) + k_B T \ln\left(\frac{p}{p^0}\right). \tag{7}$$

In general the chemical potential is given by $\mu = h - Ts$, where h is the enthalpy and s the entropy. Hence we can write

$$\mu_{gas}(T,p) = h_{gas}(T,p^0) - Ts_{gas}(T,p^0) + k_B T \ln\left(\frac{p}{p^0}\right)$$

$$= [h_{gas}(T,p^0) - h_{gas}(T=0 \text{ K},p^0)]$$

$$+ [h_{gas}(T=0\text{K},p^0) - E_{gas}]$$

$$+ E_{gas} - Ts_{gas}(T,p^0) + k_B T \ln\left(\frac{p}{p^0}\right)$$

$$= \Delta h_{gas}(T,p^0) + E_{gas}^{vib}(T=0 \text{ K}) + E_{gas}$$

$$- Ts_{gas}(T,p^0) + k_B T \ln\left(\frac{p}{p^0}\right), \tag{8}$$

where $\Delta h_{gas}(T,p^0) = h_{gas}(T,p^0) - h_{gas}(T=0 \text{ K},p^0)$ and $E_{gas}^{vib}(T=0 \text{ K})$ represents the sum of the zero-point vibration energies for the molecule.

In the presence of an atmosphere containing H$_2$S and H$_2$, sulfur may be exchanged with the MoS$_2$ stripe via the reaction

$$H_2(g) + S(*) \rightleftharpoons H_2S(g) + (*), \tag{9}$$
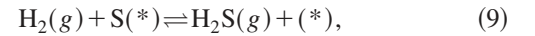
where (*) denotes a sulfur vacancy on the MoS$_2$ stripe. It is assumed that the reaction is in thermodynamic equilibrium. Assuming H$_2$S and H$_2$ to behave like ideal gases infers

$$\mu_S = \mu_{H_2S} - \mu_{H_2}$$

$$= [\Delta h_{H_2S}(T,p^0) - \Delta h_{H_2}(T,p^0)] + [E_{H_2S}^{vib}(T=0 \text{ K})$$

$$- E_{H_2}^{vib}(T=0 \text{ K})] - (E_{H_2S} - E_{H_2}) - T[s_{H_2S}(T,p^0)$$

$$- s_{H_2}(T,p^0)] + k_B T \ln\left(\frac{p_{H_2S}}{p_{H_2}}\right), \tag{10}$$

where Eq. (8) has been applied. Choosing $p^0 = 1$ bar, experimental data for $\Delta h(T,p^0)$ and $s(T,p^0)$ may be found in standard thermodynamic tables[24,23] and $E^{vib}(T=0 \text{ K})$ is estimated from experimental values for the molecular vibration frequencies.[24] In Eq. (10) it is noticed that μ_S only depends on the ratio p_{H_2S}/p_{H_2} and not on the individual partial pressures.

Next we turn our attention to the second chemical potential entering Eq. (5), μ_H. In the presence of H_2, hydrogen may adsorb on the MoS_2 stripe via the reaction
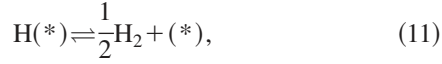
$$H(*) \rightleftharpoons \frac{1}{2} H_2 + (*), \tag{11}$$

where $(*)$ now indicates a hydrogen adsorption site on the MoS_2 stripe. Assuming the reaction to be in thermodynamic equilibrium we can write

$$\mu_H = \frac{1}{2}\mu_{H_2} = \frac{1}{2}\left[\Delta h_{H_2}(T, p^0) + E_{H_2}^{vib}(T=0 \text{ K}) + E_{H_2} \right.$$
$$\left. - Ts_{H_2}(T, p^0) + k_B T \ln\left(\frac{p_{H_2}}{p^0}\right) \right], \tag{12}$$

where Eq. (8) has been applied.

C. Range of chemical potentials

In terms of Eqs. (10) and (12) the chemical potentials for sulfur and hydrogen may be estimated. However, these quantities cannot be varied without bounds and this section deals with the estimation of these bounds.

We start by examining the range of the chemical potential for sulfur, μ_S. If it becomes too large the sulfur will prefer to form bulk sulfur and the solid state of MoS_2 becomes unstable. This upper bound can be written as

$$\mu_S \lesssim \mu_{S(bulk)} \approx E_{S(bulk)}, \tag{13}$$

where in the last term we have applied the approximation for the free energy of a solid, discussed in Sec. III A. A similar argument also applies to bulk molybdenum and leads to the lower bound. The free energy of formation for MoS_2, $\Delta G_f^{MoS_2}$, is given by

$$\Delta G_f^{MoS_2} = g_{bulk}^{MoS_2} - \mu_{Mo(bulk)} - 2\mu_{S(bulk)}. \tag{14}$$

Combining this expression with Eq. (2) yields

$$\mu_S - \mu_{S(bulk)} = \frac{\Delta G_f^{MoS_2}}{2} - \frac{1}{2}[\mu_{Mo} - \mu_{Mo(bulk)}]. \tag{15}$$

In order for MoS_2 to be stable against the formation of Mo it is required that $\mu_{Mo} - \mu_{Mo(bulk)} \geq 0$ and the lower bound then follows from Eq. (15),

$$\mu_S - \mu_{S(bulk)} \geq \frac{\Delta G_f^{MoS_2}}{2}. \tag{16}$$

An estimate for $\Delta G_f^{MoS_2}$ is obtained by approximating it with the energy of formation, $\Delta E_f^{MoS_2}$, i.e.,

$$\Delta G_f^{MoS_2} \approx \Delta E_f^{MoS_2} = E_{bulk}^{MoS_2} - E_{Mo(bulk)} - 2E_{S(bulk)}. \tag{17}$$

Using the α phase of sulfur for the evaluation of $E_{S(bulk)}$ we find $\Delta E_f^{MoS_2} = -2.58$ eV (-59.5 kcal/mol). The experimen-

tal value for the heat of formation for MoS_2 at zero temperature is given by -55.52 kcal/mol.[23] In summary the bounds on μ_S are estimated to be

$$-1.3\text{eV} \lesssim \mu_S - \mu_{S(bulk)} \lesssim 0. \tag{18}$$

Next we focus on the bounds for the chemical potential of hydrogen, μ_H. The upper limit of μ_H is determined by the point at which hydrogen will begin to condense on the MoS_2 stripe. However, for the temperatures of interest the solid phase of H_2 does not exist. An appropriate upper limit for μ_H is thus set by

$$\mu_H \lesssim \frac{1}{2} E_{H_2}, \tag{19}$$

i.e., by the energy of an isolated H_2 molecule at zero temperature. On the other hand hydrogen will only be adsorbed on the MoS_2 stripe as long as

$$N_H \mu_H \geq \min[G_{stripe}(MoS_2 + N_H H) - G_{stripe}(MoS_2)]. \tag{20}$$

The right-hand side can again be approximated by replacing G_{stripe} with the corresponding DFT energies. Next we define

$$\Delta E_H = E_{stripe}(MoS_2 + N_H H) - E_{stripe}(MoS_2) - \frac{N_H}{2} E_{H_2}. \tag{21}$$

When neglecting zero-point vibrations, ΔE_H can be identified as the total hydrogen binding energy in the zero-temperature limit. By combining Eqs. (19)–(21) we get

$$\frac{\Delta E_H}{N_H} \lesssim \mu_H - \frac{1}{2} E_{H_2} \lesssim 0. \tag{22}$$

Equation (22) indicates the range of μ_H within which hydrogen can be adsorbed on the MoS_2 stripe. The lower limit, of course, depends on the studied configuration.

D. Summary

The calculational procedure for the thermodynamic treatment can now be summarized: Equation (5) is used to calculate the edge free energy, $\gamma(\mu_S, \mu_H)$, for different edge configurations. For given μ_S and μ_H the stable structure will be the one that minimizes γ. The values of the chemical potentials can in turn be estimated through the experimental parameters, p_{H_2S}, p_{H_2}, and T, using Eqs. (10) and (12).

IV. STM ANALYSIS

The theoretical STM analysis is based on the Tersoff-Hamann formalism.[25,26] According to this treatment the tunneling matrix element between the tip and the surface is proportional to $|\psi_\nu(r_0)|^2$, where ψ_ν is an eigenstate of the investigated surface and r_0 is the position of the STM tip. This allows the tunneling current, I, to be written as
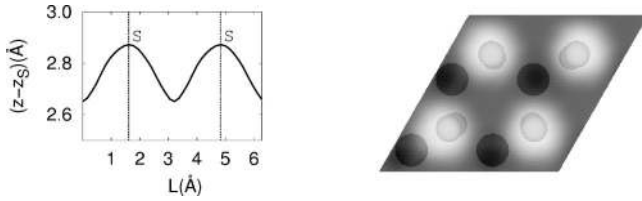
FIG. 2. An infinite slab of MoS$_2$ on Au(111). Left: The simulated line scan along the close-packed row of S atoms. The height z is measured relative to the top S layer and the corrugation is 0.22 Å. The vertical lines indicate the position of the S atoms. Right: The simulated STM image where the Au atoms have been omitted for clarity. The contour value is $\rho(\boldsymbol{r}_0, \varepsilon_F) = 8.3 \times 10^{-6}$ (Å^3 eV)$^{-1}$ and the color scale, black→white, corresponds to a variation of 0.3 Å.

$$I(U, \boldsymbol{r}_0) \propto \sum_\nu \int d\varepsilon [n_F(\varepsilon) - n_F(\varepsilon + eU)] |\psi_\nu(\boldsymbol{r}_0)|^2$$

$$\times \delta(\varepsilon + eU - \varepsilon_\nu), \tag{23}$$

where $n_F(\varepsilon)$ is the Fermi distribution function and U is the applied bias voltage. In the case of a small bias voltage Eq. (23) may be approximated by

$$I(\boldsymbol{r}_0) \propto \sum_\nu |\psi_\nu(\boldsymbol{r}_0)|^2 \delta(\varepsilon_F - \varepsilon_\nu) = \rho(\boldsymbol{r}_0, \varepsilon_F), \tag{24}$$

leading to the well-known result that a constant current STM image simply reflects an isosurface of the local density of states (LDOS) at the Fermi level, $\rho(\boldsymbol{r}_0, \varepsilon_F)$.[25,26]

We use the KS orbitals obtained from a self-consistent density-functional calculation to evaluate the tunneling matrix elements. Due to the discrete sampling of the Brillouin zone the energy levels appearing in Eq. (24) are replaced by Gaussians of finite width. However, the choice of Gaussian width is somewhat subtle and some caution is required, in particular, when examining narrow-gap semiconductors. Such a material will not be imaged in STM using a small bias voltage but if the Gaussian width exceeds the band gap an artificial nonzero LDOS and, hence, also current results. For the simulated STM images presented in this paper the Gaussian width has been carefully chosen so that only the relevant parts of the metallic bands are included. Moreover, convergence of the corrugation of the simulated STM image requires that a dense $\boldsymbol{k}$-point grid be used. The $\boldsymbol{k}$-point grids used for simulating STM images of the MoS$_2$ stripes involve a sampling rate of 0.04 Å^{-1}. This should be compared with 0.16 Å^{-1} which is used for the energetical calculations.

The contour value used to generate the STM image, i.e., the value of $\rho(\boldsymbol{r}_0, \varepsilon_F)$, is determined by matching the measured corrugation along the close-packed row of S atoms in the interior of an MoS$_2$ nanocluster with the corresponding calculated value. In the interior the effects of the edges are expected to be negligible and we model this region by an infinite MoS$_2$ slab deposited on an Au(111) substrate. [The Au(111) surface is modeled as a rigid two-layer slab assuming epitaxial growth of MoS$_2$.] The corresponding line scan and STM image are shown in Fig. 2.

Using a contour value of $\rho(\boldsymbol{r}_0, \varepsilon_F) = 8.3 \times 10^{-6}$ (Å^{3}eV)$^{-1}$ the calculated corrugation, 0.22 Å, be-

TABLE I. Experimental and calculated structural and electronic parameters for MoS$_2$. The calculated energy gaps for bulk MoS$_2$ are obtained using the experimental value for the S-Mo-S layer separation (2.975 Å).

	Experiment	DFT
Structural constants		
Hexagonal lattice constant (Å)	3.160[a]	3.22[b]
S-Mo-S layer height (Å)	3.172[a]	3.16[b]
S-Mo-S layer separation (Å)	2.975[a]	4.57[c]
Electronic constants		
Direct energy gap (eV)	1.78[a]	1.55 (1.64[b])
Indirect energy gap (eV)	1.29[a]	0.84 (1.63[b])

[a]Reference 30.
[b]Value is obtained for a single-layer MoS$_2$ slab.
[c]DFT calculation carried out with a plane-wave cutoff energy of 45 Ry.

comes equal to the experimentally measured value of 0.22 ± 0.05 Å.[27] The average height above the top S layer then becomes 2.72 Å. In Fig. 2 the simulated STM image shows the S atoms to be imaged as protrusions whereas the depressions are associated with Mo atoms. This is in agreement with previous studies of MoS$_2$.[28,29] The interaction between the Au surface and the MoS$_2$ slab will be analyzed in more detail in Sec. VI.

V. BULK MoS$_2$

As described in Sec. II bulk MoS$_2$ is a layered material. The individual S-Mo-S layers are weakly bound to each other by van der Waals forces and the unit cell consists of two such layers. They are stacked so that the Mo atoms of the upper layer are directly above the S atoms of the lower layer and vice versa. In Table I we compare calculated structural parameters for MoS$_2$ with their experimental counterparts.

It is noticed that the structural parameters for the S-Mo-S slab are in good agreement with the corresponding measured quantities. On the other hand the S-Mo-S layer separation is overestimated by 1.6 Å. This discrepancy is attributed to the fact that the van der Waals forces are poorly modeled within the applied generalized gradient approximation (PW91) for the exchange-correlation functional, see, e.g., Ref. 31. In the absence of these forces the S-Mo-S layers will be less tightly bound and the calculated DFT equilibrium distance between the layers thus becomes overestimated.

Electronically bulk MoS$_2$ is known to be a semiconductor and in Table I both the experimental and calculated values of the direct and indirect energy band gaps are shown. It is seen that the energy gaps are underestimated by the DFT calculations. This is an error often encountered within DFT using local or semilocal exchange-correlation functionals.[32] For comparison the value of the indirect band gap has previously been calculated to be 0.77 eV.[28] It is also noticed that for a single layer of MoS$_2$ the indirect band gap is almost equal to
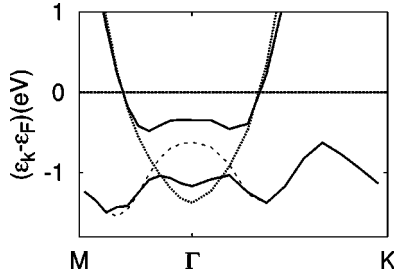
FIG. 3. Comparison of selected energy bands of an infinite single-layer MoS_2/Au(111) slab (solid) with the corresponding energy bands of the MoS_2 slab (dashed) and the Au(111) surface (dotted) separately. The Fermi level for the semiconducting MoS_2 slab is adjusted so that the valence band coincides with the valence band of the metallic MoS_2/Au(111) system close to the Brillouin-zone boundaries.

the direct band gap and is thus significantly larger than for bulk MoS_2.

VI. STM IMAGING OF MoS_2 BASAL PLANE

In the STM experiments a herringbone reconstructed Au surface[6] is used as a template for the growth of the MoS_2 nanoclusters. Hence the question arises as to whether the electronic structure of MoS_2 is strongly influenced by the presence of this substrate. Au is well known to be chemically inert[33] but clearly it must be important for the imaging of the interior of the nanoclusters since a nonzero current is measured in this region:[5] as pointed out in Sec. V an infinite sheet of MoS_2 is semiconducting with a band gap much larger than the experimentally applied bias voltage. Therefore, in the absence of Au the interior of the nanoclusters will not be imaged, disregarding effects caused by impurities.

We model the interior of the nanocluster by an infinite MoS_2 slab placed on an Au(111) surface, see also Sec. IV. The distance between the Au surface and the bottom S layer is calculated to be 2.99 Å. Selected energy bands in the two-dimensional Brillouin zone are shown in Fig. 3 along with the energy bands of MoS_2 and Au(111) separately.

Here it is seen that the valence band of MoS_2 interacts with one of the metallic Au bands. Near the edges of the Brillouin zone, K and M, the metallic band of the MoS_2/Au system resembles that of the unperturbed Au(111) surface. On the other hand, near the Γ point the shape primarily identifies with the unperturbed MoS_2 valence band which has, however, now been shifted upwards by about 0.3 eV. The opposite behavior is noticed for the valence band of the combined system. All these observations have been verified by direct inspection of the corresponding KS wave functions. The interaction between the MoS_2 slab and the Au surface thus results in an avoided crossing between the metallic Au s band and the MoS_2 valence band. This has important consequences for the electronic structure of MoS_2 at the Fermi level. Even though the metallic band at k_F will be dominated by the metallic Au state it will also have a small weight on the MoS_2 valence band. In this way the MoS_2 slab becomes weakly metallic when deposited on an Au(111) surface, and this explains that a nonzero current is measured in the inte-

rior of the MoS_2 nanoclusters. The imaging of the interior of the nanoclusters is thus an effect caused by the presence of the Au substrate.

VII. Mo EDGE

A. Edge configurations

The molybdenum-terminated ($10\bar{1}0$) edge (Mo edge) exposes a row of Mo atoms leaving the Mo edge atoms with a coordination of only four S atoms. For this reason the clean Mo edge is energetically not stable[18,34] and the Mo edge atoms prefer to be coordinatively saturated by the adsorption of additional S atoms. It has previously been reported that two configurations are feasible at the Mo edge.[18,34] They are referred to as the S dimer and the S monomer configuration and are shown in Fig. 1. Both involve the adsorption of S atoms and render the Mo atoms at the edge fully coordinated by six S atoms. The so-called S dimer configuration corresponds to adsorbing an additional row of S atoms at the edge where the S atoms are seen to form dimers in the z direction. Hence the S dimers are in registry with respect to the bulk S lattice. The S monomer configuration involves half the number of adsorbed S atoms but reconstructs in order to keep the coordination of the Mo edge atoms fixed at six. Therefore, the S monomers are shifted by half a lattice constant with respect to the S lattice, see Fig. 1. In contrast to the S dimer configuration the S monomer configuration spontaneously breaks the symmetry of the lattice along the edge introducing a superstructure with a periodicity of two lattice constants: the bond length between the S monomers and the row of Mo edge atoms varies between 1.89 Å and 1.68 Å and the Mo edge atoms themselves are found to dimerize in the x direction with an amplitude of 0.16 Å.

B. Energetics

In this section the focus will be mainly on the relative stability of the S monomer and the S dimer configurations. First the energetics is investigated in the zero-temperature limit and we then extend the results to more realistic conditions using the thermodynamic model derived in Sec. III.

Edge configurations involving a different number of S atoms are related via the reaction in Eq. (9), and the energy cost associated with the removal of a sulfur atom at $T = 0$ K is then given by

$$\Delta E_S = E[MoS_2 + (*)] + E(H_2S)$$
$$- E[MoS_2 + S(*)] - E(H_2), \quad (25)$$

neglecting the zero-point vibration energies of both the molecules and the solid. In the following we shall evaluate this quantity for the three edge terminations shown in Fig. 1. For the S monomer configuration relative to the S dimer configuration we find $\Delta E_S = -0.12$ eV/at., thus indicating that the S monomer configuration is slightly more stable than the S dimer configuration at zero temperature. On the other hand, the intermediate configuration has a positive value of ΔE_S with respect to the S dimer configuration, $\Delta E_S = 0.49$ eV. (ΔE_S relative to the S monomer configuration is, of course,
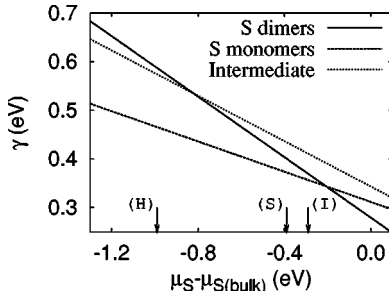
FIG. 4. The edge free energy γ as a function of the chemical potential of sulfur, μ_S, plotted for three configurations at the Mo edge (see Fig. 1): the S dimer configuration, the S monomer configuration, and the intermediate configuration. The S edge of the MoS$_2$ stripe has a coverage of 100%. The arrows indicate the values of μ_S under STM and HDS conditions, see Table II.

still negative.) This behavior is explained by the observation that the intermediate configuration does not reconstruct and hence exposes coordinatively unsaturated Mo edge atoms. In general we thus expect all intermediate configurations to be unstable relative to both the S monomer and S dimer configurations. This in turn implies that the transition from the S dimer configuration to the S monomer configuration is associated with an energy barrier and the value, $\Delta E_S = 0.49$ eV, can be taken as a minimum value for the activation energy of this reaction.

The zero-temperature results can now be extended to more realistic conditions. The edge free energy is calculated using Eq. (5) and the values for the three configurations studied above are plotted in Fig. 4 as a function of the chemical potential of sulfur, μ_S.

Since neither of these configurations involve the adsorption of hydrogen they are all independent of μ_H. The more general treatment including the possibility of hydrogen adsorption will be presented in Sec. VIII. Figure 4 shows that the atomic structure at the Mo edge is dependent on the ambient conditions and temperature, and a change of stability occurs at $\mu_S - \mu_{S(bulk)} \sim -0.21$ eV. Below this value the S monomer configuration is stable while the S dimer configuration is preferred above this point. As expected, the intermediate configuration exposing unsaturated Mo atoms is not stable at any realistic value of μ_S. We note that the results in Fig. 4 are consistent with previous work on MoS$_2$ presented in Refs. 18 and 35.

In Table II the chemical potential for sulfur is calculated for three sets of (T, p_{H_2S}, p_{H_2}) and the arrows in Fig. 4 refer to these situations.

It is noticed that S monomers are expected to be adsorbed at the Mo edge under HDS conditions. During STM imaging and sulfidation conditions, (I) and (S), μ_S is significantly higher but Fig. 4 still suggests that S monomers are adsorbed at the Mo edge. It is also noticed that μ_S during imaging is close to the transition point between the S dimer and S monomer configurations. This means that the two configurations are close in energy and the preferred structure is likely to be determined by, for example, additional interactions. Later we shall see that the presence of an Au substrate can significantly affect the position of the transition point.

C. Electronic structure

As discussed in Sec. V an infinite sheet of MoS$_2$ is semiconducting. However, terminating the MoS$_2$ slab by an Mo edge and an S edge changes the band structure significantly, see Fig. 5.

When S dimers are adsorbed at the Mo edge three bands are seen to cross the Fermi level, implying the existence of three metallic states, labeled I–III. Direct inspection of the corresponding KS wave functions reveals that I and II are localized at the Mo edge whereas III is localized at the fully covered S edge. The two metallic wave functions at the Mo edge are shown in Fig. 5. Edge state I has a Fermi wave vector of $k_F \simeq 0.39$ Å^{-1} and is seen to be almost completely localized at the S dimers. It is a superposition of p_x orbitals comprising two parallel chains along the edge. From the phase of the orbitals the two chains are noticed to be antibonding. Edge state II is seen to extend over the first three rows with $k_F \simeq 0.67$ Å^{-1}. It is primarily constituted by two bonds: (i) The d-d bond between the first row Mo atoms. From atomic projections we have found that the character of these orbitals is mainly d_{xy} and by the interatomic symmetry the corresponding Hamiltonian matrix element must be $V_{dd\pi}$.[36] (ii) The p-d bond between the two second row S atoms and the Mo atom behind. Atomic projections show that the Mo d state is dominated by $d_{x^2-y^2}$ whereas the state on the S atom is a p orbital pointing towards Mo. The bond is seen to have an even symmetry and thus the corresponding Hamiltonian matrix element is bonding $V_{pd\sigma}$.

TABLE II. The chemical potentials, μ_S and μ_H, calculated for three sets of (T, p_{H_2}, p_{H_2S}) using Eqs. (10) and (12). (I) and (S) are related to the STM experiments and represent estimates for the conditions during the imaging and synthesis of the MoS$_2$ nanoclusters (Ref. 7). During synthesis p_{H_2} is determined by the purity of the H$_2$S gas, 99.8%. For imaging the base pressure is estimated to be 1.0×10^{-13} bars corresponding to UHV and we assume that the relative amount p_{H_2S}/p_{H_2} remains constant from synthesis. The last situation, (H), represents typical working conditions for the HDS catalyst.

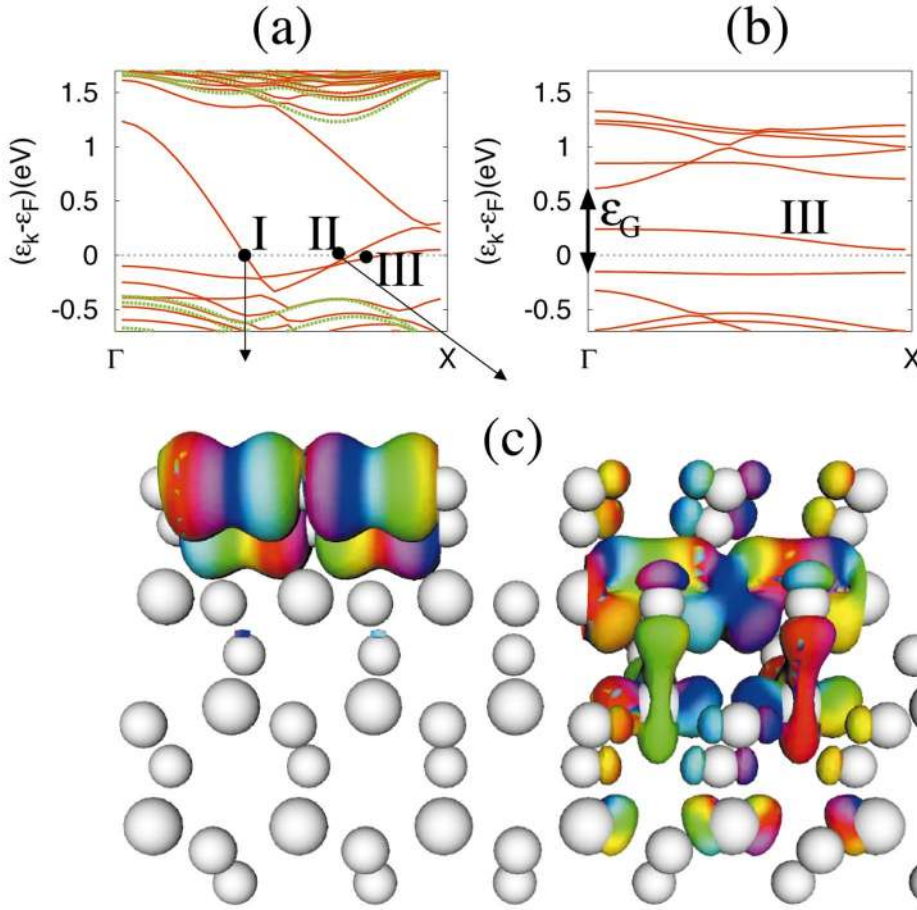|	T (K)	p_{H_2} (bars)	p_{H_2S} (bars)	$\mu_S - \mu_{S(bulk)}$ (eV)	$\mu_H - \frac{1}{2}E_{H_2}$ (eV)
(I) STM imaging	300	2.0×10^{-16}	1.0×10^{-13}	-0.29	-0.49
(S) STM sulfidation	673	2.0×10^{-12}	1.0×10^{-9}	-0.39	-1.08
(H) HDS	650	10	0.1	-0.99	-0.22

FIG. 5. (Color) One-dimensional energy bands around the Fermi level (red) for (a) a (1,12) MoS_2 stripe with S dimers adsorbed at the Mo edge and (b) a (2,6) MoS_2 stripe with S monomers adsorbed at the Mo edge. Both stripes have a fully covered S edge. The green lines represent the band structure of an infinite sheet of MoS_2. Note also that the Brillouin zone in (a) is twice as long as the one in (b). (c) Contours of the KS wave functions corresponding to the metallic states at the Mo edge. The contours are colored according to the phase of the wave functions and the rapid oscillations are due to the factor, $\exp(i\mathbf{k}_F \cdot \mathbf{r})$. The left (right), denoted I (II), corresponds to $k_F \simeq 0.39$ Å^{-1} ($k_F \simeq 0.67$ Å^{-1}) as indicated by the arrows.

Below the Fermi level the energy band of edge state I is seen in Fig. 5 to extend into the region of the MoS_2 bulk states. There the edge state may have a nonzero overlap with the bulk states. Due to this interaction hybrid bonding and antibonding states are formed resulting in an avoided crossing between the edge-state band and the bulk-state band. For this reason the edge states are in general expected to only exist within the MoS_2 band gap. A similar behavior is known for intrinsic surface states that emerge within the band gaps of bulk crystals.[37] When a surface-state band crosses the boundaries of this region it hybridizes with the bulk states and forms a so-called surface resonance.

In Fig. 5 the band structure of the Mo edge with S monomers adsorbed is also shown. There the number of metallic states is noticed to be one. Since the MoS_2 stripe has a fully covered S edge the metallic state, labeled III, can readily be identified with the metallic S edge state [also labeled III in Fig. 5(a)]. Still, the band structures of the two metallic edge states, III in Figs. 5(a) and 5(b), are noticed not to be completely identical, but a discussion of this difference is postponed to Sec. IX C. Returning to the Mo edge this means that there are no metallic edge states associated with this edge and it is thus rendered semiconducting by the S monomers. However, this observation does not necessarily exclude the existence of nonmetallic edge states. Indeed, the presence of such states is inferred by the reduced band gap. In Fig. 5(b) the transition between the edge-state conduction band and the edge-state valence band is indicated. The energy gap

is found to be 0.77 eV and this value is significantly smaller than the calculated direct bulk band gap of 1.64 eV (see Table I).

D. STM imaging

We have simulated STM images of both the S dimer configuration and the S monomer configuration. The former is shown in Fig. 6(a) and it is seen that a bright brim extends in the row behind the S dimers.

The S dimers are also imaged clearly but there the protrusions are not associated with the S atoms themselves but appear in the interstitial region. This implies that in terms of the protrusions of the basal plane the protrusions at the edge are shifted by half a lattice constant. (It is remembered from Sec. VI that the S lattice and the protrusions in the bulk region coincide.) Next we focus on the imaging of the S monomer configuration. Since neither of the edge states are metallic the tunneling current is expected to be zero for a small bias voltage. However, by applying a voltage beyond the band gap tunneling states become available and in Fig. 6(b) a simulated STM image of the S monomer configuration is shown for $U = -0.18$ V. Here the presence of a bright brim that also extends in the row behind the S monomers is noticed. The protrusions of the brim are located at the S atoms but as the underlying atomic structure they display superstructure with a periodicity of two lattice constants. Moreover, the S monomers are noticed to be imaged very
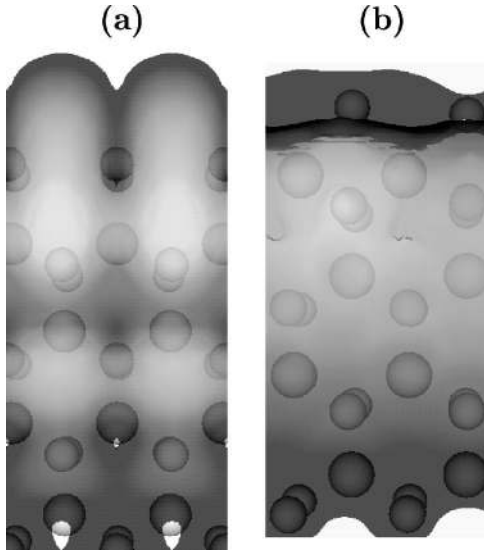
FIG. 6. Simulated STM images for (a) a (1,12) MoS$_2$ stripe with S dimers adsorbed at the Mo edge and (b) a (2,6) MoS$_2$ stripe with S monomers adsorbed at the Mo edge. The contour value for (a) is $\rho(r_0,\varepsilon_F)=8.3\times10^{-6}$ (Å^3 eV)$^{-1}$. For the S monomers the STM topograph is calculated using Eq. (23) with $U=-0.18$ V. The contour value is determined by -0.18 eV$\times\rho(\varepsilon_F,r_0)=-1.5\times10^{-6}$ Å^{-3}. Both color scales correspond to a corrugation of 1.5 Å.

weakly. In summary these characteristic features should make the S monomer and S dimer configurations clearly distinguishable in a STM and will be the subject of a forthcoming publication.[38]

E. Interaction with Au substrate

In Sec. VI we found that the presence of a metallic Au(111) surface has important consequences for the electronic structure of the insulating MoS$_2$ slab. In this section we shall study the influence of Au on the Mo edge. First the energetics of the edge is studied and we then investigate the interaction between the Au states and the metallic edge states.

In order to investigate the influence of Au we have carried out DFT calculations for a (1,6) MoS$_2$ stripe adsorbed on an Au(111) surface with both S dimers and S monomers adsorbed at the Mo edge. The relative sulfur binding energy between these configurations, ΔE_S, is now found to be 0.19 eV per S atom. This implies that in the presence of the Au substrate the S dimer configuration has now become the most stable structure at the Mo edge at zero temperature. Comparing with the sulfur binding for the isolated edge, $\Delta E_S = -0.12$ eV, the change of stability is 0.31 eV. A portion of this energy difference, however, derives from the size of the applied supercell. Since the unit vector in the x direction of the MoS$_2$/Au system has the length of a single lattice constant the S monomers cannot achieve their lowest-energy configuration where the Mo edge atoms form dimers, as described in Sec. VII A. The energy gain associated with this superstructure is estimated to be 0.09 eV for the isolated Mo edge. The zero-temperature results can now be extended to
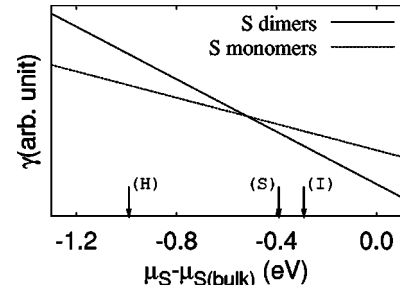

FIG. 7. (1,6) MoS$_2$ stripe on Au(111). The edge free energy γ as a function of the chemical potential of sulfur, μ_S, shown for two different configurations at the Mo edge: the S dimer configuration and the S monomer configuration. The MoS$_2$ stripes have a fully covered S edge. The arrows indicate the values of μ_S under STM and HDS conditions, see Table II.

more realistic conditions and in Fig. 7 the edge free energies of the S dimer and S monomer configurations in the presence of an Au substrate are compared.

Here it is clearly seen that the Au(111) substrate influences the structural stability of the Mo edge, cf. Fig. 4. The transition point between the two edge terminations has moved from $\mu_S-\mu_{S(bulk)}\sim-0.21$ eV for the isolated MoS$_2$ edge to -0.52 eV in the presence of the Au substrate. These changes are important for the STM experiment where the S dimer configuration is now noticed to be the most stable structure. In fact, this is the case during both imaging and sulfidation, (I) and (S), respectively. On the other hand the S monomer configuration is still clearly preferred under HDS conditions.

We now proceed to investigate the influence of Au(111) on the electronic structure of the Mo edge with emphasis on the S dimer configuration. In Fig. 8 we compare for this edge
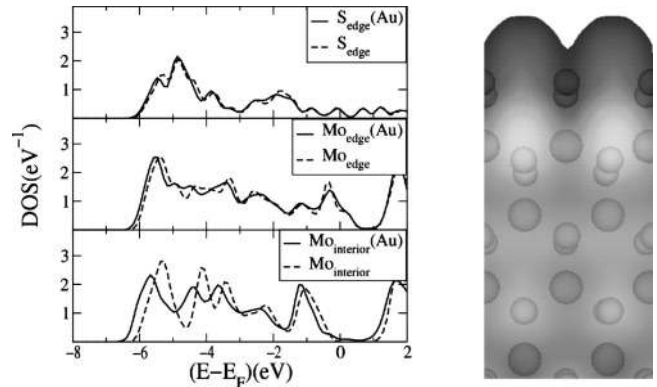

FIG. 8. MoS$_2$/Au(111) with S dimers adsorbed at the Mo edge. Left: Atom projected density of states (ADOS) for selected atoms in the MoS$_2$ stripe: the top S atom in the S dimer (S$_{edge}$), the Mo atom at the edge (Mo$_{edge}$), and a Mo in the interior of the stripe (Mo$_{int}$). The ADOS is calculated by first projecting the localized set of atomic orbitals on the self-consistent Kohn-Sham wave function and then adding the contributions from all the orbitals situated on the same atom. Right: simulated STM image for a (1,6) MoS$_2$ stripe. For clarity the Au atoms have not been retained. The contour value is $\rho(r_0,\varepsilon_F)=8.3\times10^{-6}$ (Å^3 eV)$^{-1}$ and the color scale corresponds to a corrugation of 1.5 Å.

termination the atom projected density of states (ADOS) calculated for three different atoms in the MoS_2 stripe with and without an underlying Au surface.

In general, it is seen that the interaction with the electronic Au states causes a broadening of the features in the ADOS as well as a small shift down in energy. For the S and Mo atoms at the Mo edge the electronic structure at the Fermi level remains essentially unchanged thus indicating that the metallic edge states are only weakly perturbed by the presence of Au. However, as expected from the discussion in Sec. VI the ADOS for the Mo atom in the interior of the MoS_2 stripe becomes nonzero within the intrinsic band gap of bulk MoS_2. These trends are also reflected in the simulated STM image for the S dimer configuration shown in Fig. 8. It is seen that the imaging of the metallic states localized at the edge is essentially unchanged by the presence of Au. When moving away from the edge the interaction with the substrate becomes clear, cf. Fig. 6(a). The LDOS at the Fermi level is now nonzero and the S atoms (Mo atoms) are imaged as protrusions (depressions). These observations are in agreement with the simulated STM image for the infinite MoS_2/Au system shown (see Fig. 2).

VIII. ADSORPTION OF HYDROGEN

It is well known that the basal plane of MoS_2 is chemically not very active. Experimentally it has been shown that organic molecules such as thiophene and butene only adsorb there at cryogenic temperatures.[39] Moreover, based on a DFT study Byskov *et al.* have reported[34] that hydrogen cannot form stable bonds with the MoS_2 basal plane. This indicates, as is generally accepted, that the chemically active sites in HDS must be associated with the edges and a few previous studies have therefore focused on the reactivity of the edges towards hydrogen.[40–42]

As discussed in Sec. VII A the Mo edge atoms are fully coordinated when either of the two stable configurations, S dimers or S monomers, is present. This immediately suggests that the Mo edge is chemically inert. However, the electronic structure at the Mo edge is also influenced by the presence of edge states. These states may interact with the adsorbates and form stable chemical bonds. It should be stressed that the origin of such bonds will not be of a localized nature that can be accounted for by simple electron counting.

In the following we shall study the adsorption of atomic hydrogen at the Mo edge. The reason for this is twofold: first hydrogen may be regarded as a simple probe testing the chemical activity of the edges. Second, hydrogen is abundant under HDS conditions and during sulfidation of the MoS_2 clusters in the STM experiment. In relation to the HDS process the dissociative adsorption of hydrogen is important. It is often referred to as hydrogen activation and the activated hydrogen can then react with the sulfur atom of an adsorbed organic compound.

First the atomic structure for a number of different adsorption sites will be presented and we then extend the thermodynamic treatment of Sec. VII B to include the possibility for hydro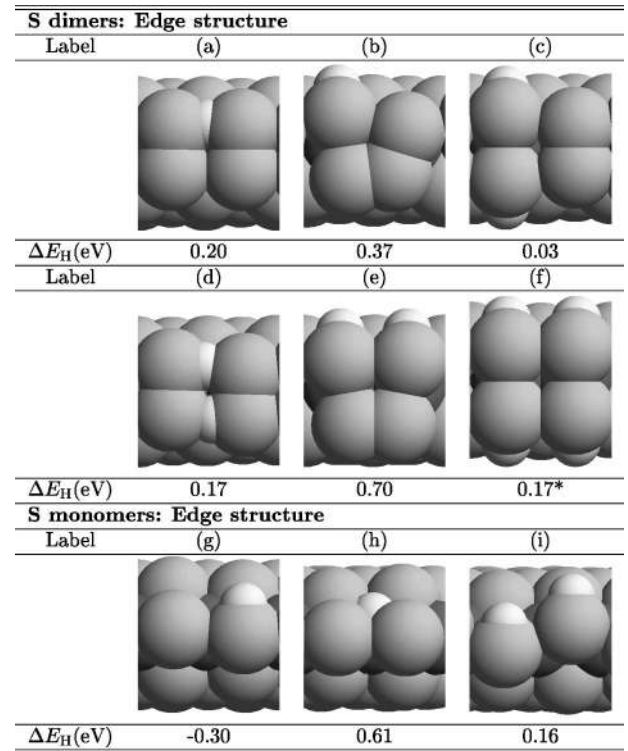gen adsorption at the Mo edge. Finally, the influence of hydrogen on the electronic structure and STM imaging is discussed.

FIG. 9. The investigated Mo edge adsorption sites for hydrogen and their calculated binding energies, ΔE_H. The configurations are viewed from the side of the Mo edge. Each configuration represents a (local) minimum on the potential-energy surface for hydrogen. We note that the calculations are performed with a (2,6) [*=(1,12)] MoS_2 stripe.

A. Adsorption sites

A number of different adsorption sites for hydrogen have been found at both the S dimer and S monomer configurations. These sites are identified by first placing hydrogen in a number of different initial configurations. Then all atomic coordinates are relaxed according to the calculated forces and in this way a (local) minimum on the potential-energy surface for hydrogen is obtained. The atomic structures thus found are listed in Fig. 9 along with the calculated values for ΔE_H, see Eq. (21).

Here it is seen that only a single site is associated with an energy gain, $\Delta E_H < 0$. A weak bond, the configuration of Fig. 9(g), may be formed with the Mo edge when H adsorbs on every second S monomer. On the other hand, there are no stable configurations associated with the S dimer configuration. From Fig. 9 it is seen that three hydrogen configurations at this edge structure have ΔE_H close to zero, Figs. 9(c), 9(d), and 9(f), and the binding energies per H atom are only separated by 0.07 eV. One of them is seen to involve the adsorption of two hydrogen atoms between the S dimers and the two others have H adsorbed atop both sides of the S dimers. For the two latter ones the adsorption of hydrogen causes the S dimers to split into two S-H groups. However,
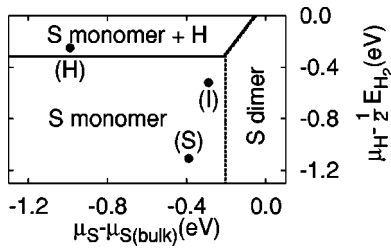
FIG. 10. The stable configurations at the Mo edge for realistic values of μ_S and μ_H. The labels refer to the three experimental situations listed in Table II.

in thermodynamic equilibrium neither of these configurations is expected to be stable and hence only the configuration of Fig. 9(g) is likely to exist at the Mo edge. This result also indicates that the S monomer configuration in general is chemically more active than the S dimer configuration.

B. Thermodynamic treatment

In Sec. VII B the relative stability of the S monomer and the S dimer configurations was examined in thermodynamic equilibrium. We now extend this treatment to also include the possibility for hydrogen adsorption and the edge free energy then becomes dependent on both μ_S and μ_H. Since the stable structure will be the one that minimizes the edge free energy, γ, we can plot a diagram indicating the preferred structure for realistic values of μ_S and μ_H. Such a diagram is shown in Fig. 10.

Here it is seen that by allowing for the adsorption of H on the MoS$_2$ stripe a new stable structure emerges for high values of μ_H. This structure corresponds to the configuration in Fig. 9(g) where a hydrogen atom is adsorbed on every second S monomer. In Fig. 10 the points (I) and (S) indicate the positions of the chemical potentials during the STM experiment. Due to their low value of μ_H the adsorption of hydrogen at the Mo edge is seen not to be relevant under these conditions. Under HDS conditions, however, the chemical potential is right above the transition line where hydrogen will start to adsorb at the S monomers. This suggests that in this regime hydrogen is abundant at the edge in the form of S-H groups. The presence of hydrogen will also influence the electronic structure, and this issue will be addressed in more detail in the next section.

C. Electronic structure and STM imaging

In Sec. VIII B it was established that in thermodynamic equilibrium the configuration, where hydrogen is adsorbed on every second S monomer, may be realized for large values of μ_H. In fact, this configuration was predicted to be observed under HDS conditions and its electronic structure must thus be important for understanding the catalytic properties of the Mo edge. In Fig. 11 it is seen that two metallic edge states exist.

The edge state labeled III is readily identified with the metallic edge state localized at the S edge. The other metallic state labeled I_H is localized at the Mo edge. This shows that the adsorption of hydrogen changes the Mo edge from semi-
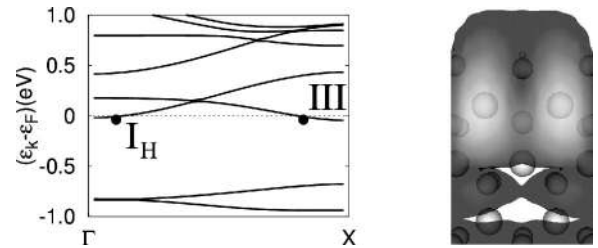

FIG. 11. A (2,6) MoS$_2$ stripe with S monomers + H adsorbed at the Mo edge, see the configuration in Fig. 9(g), and a fully covered S edge. Left: the band diagram for energies around the Fermi level. Right: simulated STM image with $\rho(\varepsilon_F, r_0) = 8.3 \times 10^{-6}$ (eV Å^3)$^{-1}$. The color scale corresponds to a corrugation of 1.5 Å.

conducting to metallic. The metallic edge state is noticed to have a low occupation with $k_F = 0.07$ Å^{-1}. A simulated STM image of the Mo edge is also shown in Fig. 11. Like the STM images for the S monomer and S dimer configurations it is seen to have a bright brim extending along the row behind the adsorbates at the edge. However, the protrusions of the bright brim are now located at the Mo atoms. This implies that they will appear out of registry with the S lattice and thus with the protrusions in the bulk region. Moreover, the interstitial region between the S monomers is seen to be imaged rather than the S monomers themselves. This in turn implies that the protrusions at the edge will be in registry with the protrusions of the basal plane. In summary these characteristic features should make the S monomer + H configuration clearly distinguishable from the clean S dimer and S monomer configurations using STM.

Next we focus on the S dimer configuration at the Mo edge. According to Sec. VIII B hydrogen is not expected to adsorb at this structure in thermodynamic equilibrium. However, experimentally MoS$_2$ clusters with S dimers adsorbed at the edges[5] have been exposed to doses of reactive H atoms.[43] This, of course, changes the binding energies for the hydrogen dramatically. In order to evaluate this new binding energy the term in Eq. (21), $N_H E_{H_2}/2$, should be replaced by $N_H E_H$, where E_H is the DFT energy for an isolated H atom. For the configurations Figs. 9(c), 9(d), and 9(f) the hydrogen binding energies now become $\Delta E_H = -4.51$ eV (0.03 eV), -4.37 eV (0.17 eV), and -8.93 eV (0.17 eV), respectively. (In parentheses the binding energies in the presence of H$_2$ are indicated.) This shows that the configuration in Fig. 9(f) where H atoms are adsorbed on both sides of every S dimer becomes by far the most stable configuration, the reason being that this structure is the one that can bind the most H atoms per unit edge length. The associated band structure is shown in Fig. 12.

Comparing with the clean S dimer configuration it is seen that the number of metallic bands has remained constant, and the influence of hydrogen is simply to induce a small shift in energy of the two metallic bands at the Mo edge. As seen in Fig. 12 the imaging of the edge is also essentially unchanged, cf. Fig. 6, retaining all the characteristic features of the clean edge.
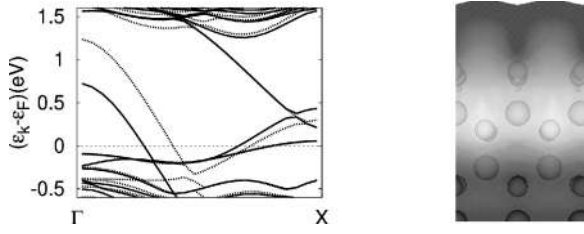
FIG. 12. A (1,12) MoS_2 stripe with S dimers and hydrogen adsorbed at the Mo edge, see the configuration in Fig. 9(f), and a fully covered S edge. Left: the band diagram for energies around the Fermi level with (solid) and without (dotted) hydrogen adsorbed. Right: simulated STM image with $\rho(\varepsilon_F, r_0) = 8.3 \times 10^{-6}$ $(eV\ Å^3)^{-1}$. The color scale corresponds to a corrugation of 1.5 Å.

IX. S EDGE

A. Edge configurations

The sulfur-terminated ($\bar{1}010$) edge, the S edge, exposes a row of S atoms. This configuration, shown in Fig. 1, is referred to as the fully covered S edge. It clearly breaks the symmetry of the S lattice along the edge: the S edge atoms form dimers and every second S dimer is pointing either up or down. The Mo atoms in the row behind are also found to dimerize in the x direction with a small amplitude of 0.1 Å. We have estimated the energy gain associated with this wobbling to be 0.23 eV. Vacancies can also be formed by removing S atoms from the edge. In contrast to the Mo edge neither of these configurations reconstructs. Hence having a coverage below 100% automatically implies the presence of coordinatively unsaturated Mo atoms. Two examples of such configurations are shown in Fig. 1 indicating the atomic structure of the 75% and 50% covered S edge.

B. Energetics

As for the Mo edge the different edge configurations at the S edge are related via the reaction in Eq. (9). We find for the 75% covered S edge that $\Delta E_S = 0.23$ eV, see Eq. (25), relative to the fully covered S edge. Moreover, the removal of an additional S atom thus achieving a coverage of 50% yields $\Delta E_S = 0.64$ eV. Therefore the creation of a vacancy and thus the exposure of unsaturated Mo atoms is an activated process and it becomes energetically increasingly expensive to remove additional S atoms. However, comparing these values with the formation energy of a single unsaturated Mo atom at the Mo edge, $\Delta E_S = 0.49$ eV, we see that unsaturated Mo atoms are more easily accessible at the S edge. For this reason the S edge is expected to be chemically more active than the Mo edge, and this difference is, of course, important for the HDS process.

A number of adsorption sites for hydrogen has also been identified at the S edge using the same procedure as in Sec. VIII A for the Mo edge. Figure 13 displays the investigated configurations along with their calculated values for the hydrogen binding energy, ΔE_H.

In general, it is seen that the hydrogen bonds formed at the S edge are stronger than those at the Mo edge, cf. Fig. 9.

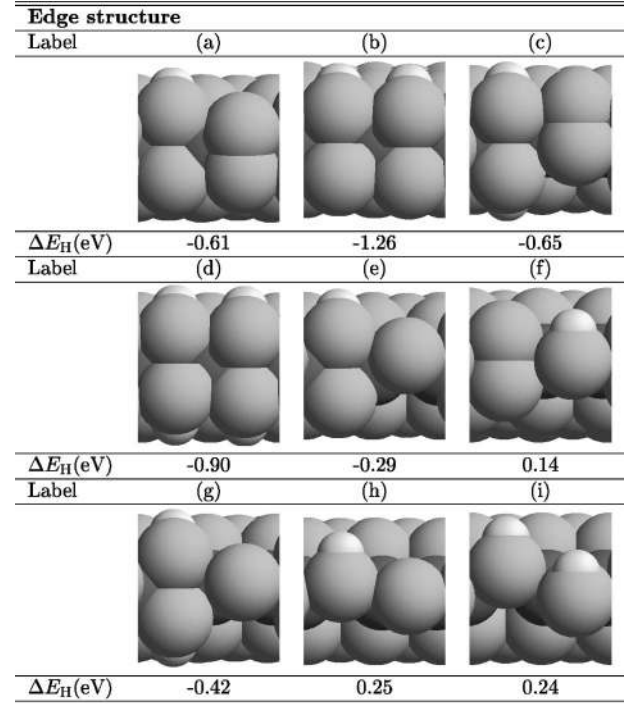| Edge structure			
Label	(a)	(b)	(c)
ΔE_H(eV)	−0.61	−1.26	−0.65
Label	(d)	(e)	(f)
ΔE_H(eV)	−0.90	−0.29	0.14
Label	(g)	(h)	(i)
ΔE_H(eV)	−0.42	0.25	0.24

FIG. 13. The investigated S edge adsorption sites for hydrogen and their calculated binding energies, ΔE_H. The configurations are viewed from the side of the S edge. Each configuration represents a (local) minimum on the potential-energy surface for hydrogen. We note that the calculations have been performed with a (2,6) MoS_2 stripe.

Having a coverage of 50% Fig. 13 shows that ΔE_H is always positive indicating that stable hydrogen will not be present at low coverages ($\leqslant 50\%$). On the other hand, hydrogen may form stable bonds, $\Delta E_H < 0$, with the fully covered S edge. The adsorption of hydrogen causes the S dimer to split creating one or two S-H groups. In Fig. 13 it is noticed that the configuration of Fig. 13(b), where two H atoms are adsorbed on top of the two S dimers of a fully covered S edge, yields the strongest binding energy. In fact, the energy gain associated with the addition of two H atoms, see the configuration 13(d), is large and negative. For the 75% covered S edge two stable configurations are seen to exist, the configurations Figs. 13(e) and 13(g), having an energy difference of only 0.13 eV. Hence both structures are likely to exist for this coverage and their relative stability will depend on the temperature and partial pressure of hydrogen.

These results can now be extended to more realistic conditions by application of the thermodynamic model. In Fig. 14 is shown a diagram for the S edge indicating the stable structures for realistic values of μ_S and μ_H.

It is seen that four different structures may be present: at high values of μ_S and low values of μ_H having 100% coverage yields the lowest edge free energy. However, by decreasing μ_S the creation of vacancies becomes more favored and at $\mu_S - \mu_{S(bulk)} \sim -0.56$ eV there is a change of stability. Below this value the 75% covered S edge is more stable. Reducing μ_S further an additional vacancy is created at $\mu_S - \mu_{S(bulk)} \sim -0.97$ eV resulting in a coverage of 50%. It
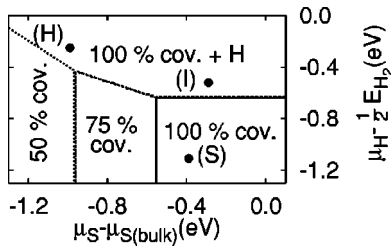
FIG. 14. A diagram indicating the stable structures at the S edge for different values of (μ_S, μ_H). The labels refer to the three experimental situations listed in Table II.

should be emphasized, though, that for the real S edge the coverage will not be reduced in steps of 25% but rather decrease continuously from a coverage of 100% as μ_S is lowered. The stepwise reduction stems from the finite size of the unit cell parallel to the edge. Now, having a high value of μ_H stabilizes the fully covered S edge and hydrogen will adsorb as shown in the configuration of Fig. 13(b). Due to the large energy gain associated with this structure, the configurations Figs. 13(e) or 13(g) do not become stable for any realistic value of μ_S. In fact, as indicated by (H) in Fig. 14(b), the configuration is expected to be stable even under HDS conditions. (I) and (S) refer to the imaging and sulfidation conditions, respectively, during the STM experiment. It is seen that if an S edge is exposed a fully covered edge will be synthesized under sulfidation, but as imaging conditions are achieved hydrogen adsorption at the edge becomes favored.

C. Electronic structure

In this section we focus on the fully covered S edge with or without hydrogen adsorbed. The one-dimensional energy bands for these structures are shown in Fig. 15.

For both systems the presence of three metallic states, denoted I, II, and III (III$_H$), is noticed. Since the MoS$_2$ stripes both have S dimers adsorbed at the Mo edge, the states I and II are readily identified with the two one-dimensional, metallic edge states localized at the Mo edge. [Because the supercell contains two rows of Mo atoms in the x direction, II is seen to be zone folded, cf. Fig. 5(a).] Direct inspection of the remaining states III and III$_H$ reveals that they are both localized at the S edge. For the clean S edge, III is seen in Fig. 15 to approach the Fermi level when moving towards the Brillouin-zone boundary without actually crossing it. A difference compared to Fig. 5 is noticed: there the energy band of the edge state III is seen to cross the Fermi level. This derives from the superstructure displayed by the fully covered S edge. Since the calculation presented in Sec. VII C was performed with a supercell containing only a single row of Mo atoms it did not allow for the superstructure to be formed. The difference between the two bands thus reflects the changes caused by the wobbling of the fully covered S edge. Adsorbing H on the S dimers changes the band structure of the S edge state, now denoted III$_H$. Figure 15 shows that the edge state has become truly metallic and crosses the Fermi level at $k_F \simeq 0.15$ Å^{-1}.

Contour plots of the metallic edge states III and III$_H$ are also displayed in Fig. 15. For the clean S edge the edge state III is characterized by two chemical bonds: the d-d bond between the first row Mo atoms and the p-d bond between the same Mo atoms and the S atoms at the edge. Like the atomic structure, the bonds exhibit a periodicity of two along the edge. The d-d bond is seen to be between the Mo atoms that belong to different dimers. In contrast, the Mo atoms only couple with the S dimers located in the direction of the dimerization. Turning to the other metallic edge state III$_H$, it is generated when H adsorbs on top of every S edge atom. Figure 15 shows that it is primarily characterized by the bond between the p orbital on the lower S atom at the edge
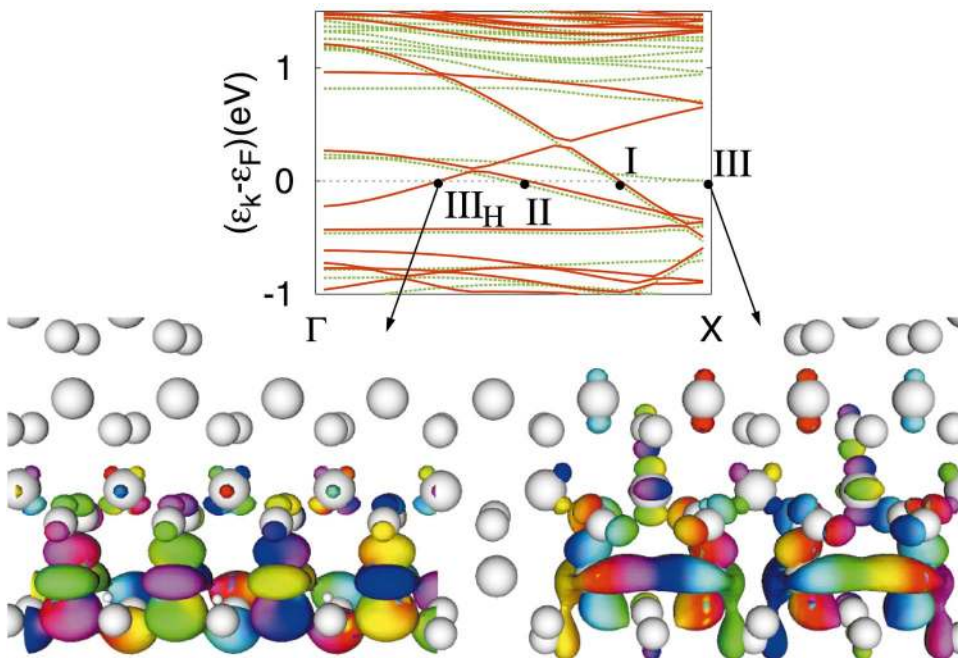

FIG. 15. (Color) Top: Comparison of the one-dimensional energy bands at the Fermi level for a (2,6) MoS$_2$ stripe having a fully covered S edge with [red, the configuration in Fig. 13(b)] and without H adsorbed [green, 100% coverage in Fig. 1]. The MoS$_2$ stripes have S dimers adsorbed at the Mo edge. Bottom: Contours of the KS wave functions corresponding to the one-dimensional, metallic edge states at the S edge. The left (right), labeled III (III$_H$) as indicated by the arrow, has $k_F \simeq 0.49$ Å^{-1} ($k_F \simeq 0.15$ Å^{-1}).
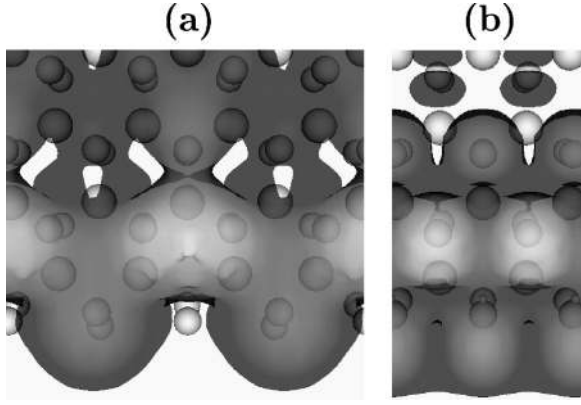
FIG. 16. Simulated STM images for (a) a (2,6) MoS_2 stripe with a fully covered S edge and (b) a (1,12) MoS_2 stripe with configuration (b) at the S edge. $\rho(r_0, \varepsilon_F) = 8.3 \times 10^{-6}$ $(\text{Å}^3 \text{ eV})^{-1}$ is used as the contour value and the color scale corresponds to a corrugation of 1.5 Å.

and the Mo d orbital in the row behind. The corresponding Hamiltonian matrix element is seen to be $V_{pd\pi}$.

D. STM imaging

STM images have been simulated for the fully covered S edge with and without hydrogen. They are displayed in Fig. 16 and for the fully covered S edge the following characteristic features are noticed. A bright brim is seen to extend in the row behind the edge. As the underlying atomic structure it displays a clear superstructure with a periodicity of two lattice constants. This periodicity is also retained at the outer row of S atoms where only the elevated S dimers are imaged. The simulated STM image for the fully covered S edge has the periodicity of the lattice, see Fig. 16(b). It has a bright brim that extends in the row behind the edge. Furthermore, the S–H groups are noticed to be imaged clearly. In summary these characteristic features should make the two configurations clearly distinguishable in STM.

X. EFFECTS CAUSED BY FINITE-SIZE EDGES

The theoretically studied MoS_2 stripes have infinite edges and it is certainly possible that when such stripes are terminated by corners, changes in both the electronic and atomic

structure of the edges may occur. This section is devoted to a study of these effects where the emphasis will be on the Mo edge with S dimers adsorbed.

In order to investigate the finite-size effects we have carried out DFT calculations for small MoS_2 triangles. The calculational details are presented in Sec. X A and the electronic and structural changes caused by the triangular shape are then studied in the subsequent section.

A. Calculational details

We have carried out DFT calculations for three differently sized MoS_2 triangles, all exposing the Mo edge with S dimers adsorbed. The islands have $N = 4-6$ S dimers adsorbed along the edges. Each supercell contains a single MoS_2 triangle and the repeated triangles are separated by approximately 10 Å.[44]

At the corners of the MoS_2 triangles a number of different atomic structures are feasible. We have investigated three different configurations with either an S dimer, an S monomer, or a vacancy present at the corner Mo atom. The sulfur binding energy is calculated using Eq. (25) and we find that the vacancy corresponds to the energetically most stable configuration. This result is not surprising since a vacancy renders the corner Mo atom coordinated by six S atoms.

B. Electronic and structural effects

We first focus on the $N = 4$ MoS_2 triangle shown in Fig. 17. Inspection of the electronic structure around the Fermi level reveals the presence of three states that are reminiscent of the metallic S dimer state, referred to as edge state I in Sec. VII C. Their eigenvalues are $\varepsilon = -0.10$ eV, 0.06 eV, and 0.06 eV and the wave functions are shown in Figs. 17(a)–17(c).

The triangle has a C_3 symmetry and the state of Fig. 17(a) can thus be identified with the A representation of this group. On the other hand the two degenerate states belong to the two-dimensional E representation.

In order to understand the underlying physics we adopt a simple tight-binding picture. This is justified by the observation that the energy band of the metallic S dimer state for the infinite edge, see Fig. 5, is seen to closely resemble the well-known shape of a one-dimensional tight-binding band,
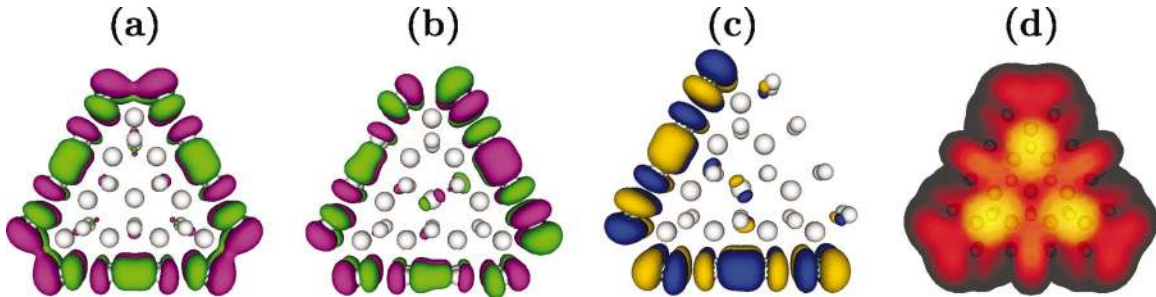

FIG. 17. (Color) $N = 4$ MoS_2 triangle. (a)–(c) show contours of the KS wave functions for the S dimer states. The eigenvalues are $\varepsilon = -0.10$ eV, 0.06 eV, and 0.06 eV and the contours are colored according to the phase of the wave functions. (d) shows a simulated STM image. $\rho(r_0, \varepsilon_F) = 8.3 \times 10^{-6}$ $(\text{Å}^3 \text{ eV})^{-1}$ is used as the contour value and the Gaussian width is set to 50 meV. The color scale corresponds to a corrugation of 2.0 Å.
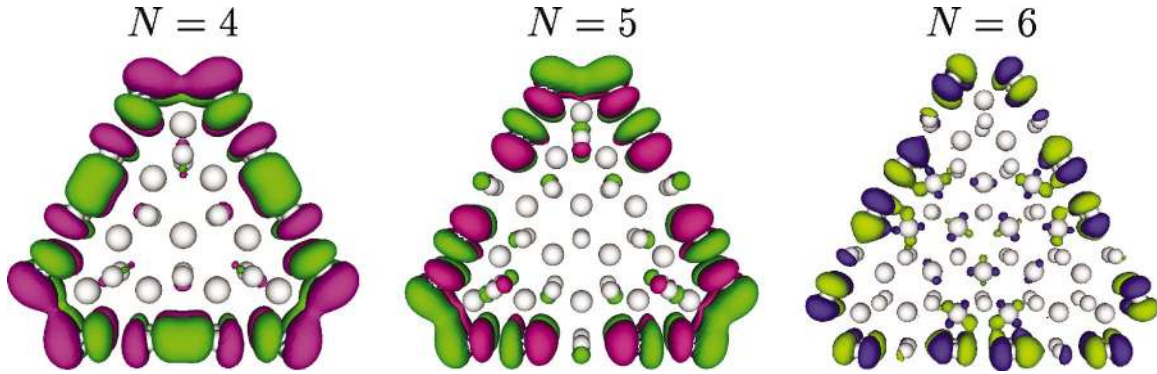
FIG. 18. (Color) Contours of the KS wave functions representing the S dimer states for $N=4-6$. The eigenvalues are -0.10 eV, 0.31 eV, and -0.07 eV, respectively, relative to the Fermi level, and the contours are colored according to the phases.

$\varepsilon(k)=\varepsilon_0+2t_{\text{edge}}\cos(k)$, where ε_0 is the center of the band and t_{edge} is the hopping matrix element between neighboring S dimers. With this identification we estimate t_{edge} to be of the order of 1 eV. The energy splitting of the S dimer states in Fig. 17, $\delta\varepsilon\sim0.1$ eV, can then be taken as the measure for the hopping matrix element between the different edges, t_{corner}. This implies that at the corners of the MoS$_2$ triangle the hopping matrix elements are an order-of-magnitude smaller than along the edges. t_{corner} thus only needs to be treated as a first-order perturbation connecting the three otherwise isolated, finite chains of S dimers. In Fig. 17 the phase of the p orbitals is noticed to change by π between the two central S dimers. Following the lines of the discussion above this pattern can be understood within a tight-binding picture: the S dimer states extending along the individual edges may simply be regarded as eigenstates of the finite tight-binding Hamiltonian.

We shall now study how the triangular shape influences the STM imaging. Since the MoS$_2$ triangles are of finite size they will have a discrete excitation spectrum. At small bias voltages Eq. (24) applies but due to thermal smearing, states that are approximately within the range of $k_B T$ of the Fermi level will contribute to the current. In Fig. 17(d) a simulated STM image of the $N=4$ MoS$_2$ triangle is shown. For this image the Gaussian width is set to 50 meV. It is seen that the effects of the corner discussed above are also clear from the STM image in Fig. 17(d) where the interstitial regions between the two central S dimers are noticed to have more pronounced protrusions. This is explained by the observation that when there is a change of phase by π between two neighboring p orbitals, the lobes in the interstitial region will begin to interfere constructively instead of destructively. Consequently, this region will also have more pronounced images.

In the following we discuss how this effect carries over to larger triangles. In Fig. 18 the singlet S dimer states closest to the Fermi level are shown for $N=4-6$.

Again it is noticed that the corners introduce standing wave patterns along each of the edges. However, for $N=6$ a small structural relaxation of the S dimers is also observed. Along each edge the S dimers are found to form two groups of trimers. Such a structural relaxation will also influence the STM imaging. In general, it is expected that if the distance

between two dimers is decreased the overlap between the p orbitals is changed: the destructive interference between the lobes of these orbitals becomes stronger and the resulting intensity of the protrusion is weakened. The opposite effect will, of course, be relevant when the distance between two S dimers is increased. Recently Schweiger and co-workers have presented calculations for larger MoS$_2$ triangles having up to ten S dimers adsorbed along each edge.[35] For this size of triangles they report the S dimers to show a weak pairing parallel to the edge. According to the discussion above and in agreement with a simulated STM image of the MoS$_2$ triangle, see Ref. 35, the resulting protrusions along the Mo edge show a superstructure where every second protrusion is imaged more clearly than its two neighbors. Our DFT calculations for the $N=6$ MoS$_2$ triangle have shown a similar pairing for the S dimers along a single edge. This configuration is, however, metastable with an energy difference of 0.54 eV to the unpaired stable structure. We stress that the pairing of the S dimers must be an effect caused by the finite length of the MoS$_2$ edges, and based on the investigation of the MoS$_2$ stripes the pairing is expected to disappear in the limit of an infinite MoS$_2$ edge.

XI. RELATION TO STM EXPERIMENTS

In this section we will relate the theoretical analysis presented in this paper to a recent STM experiment on MoS$_2$.[8] First we briefly outline the details of the STM experiment and give a description of the recorded STM images. The experimental images are then compared with their simulated counterparts. Finally, the STM experiment is discussed in relation with the thermodynamic treatment.

The STM experiment is performed in ultrahigh vacuum (UHV) using a reconstructed Au(111) surface as a template. Triangular shaped, single-layer MoS$_2$ islands are then synthesized on the substrate with the parameters given in Table II. For imaging the temperature is lowered to 300 K and UHV conditions are achieved. The STM images are recorded in constant current mode with a bias voltage in the mV range. For more experimental details, see Ref. 7. An experimental STM image of a single-layer MoS$_2$ triangle is shown in Fig. 19.

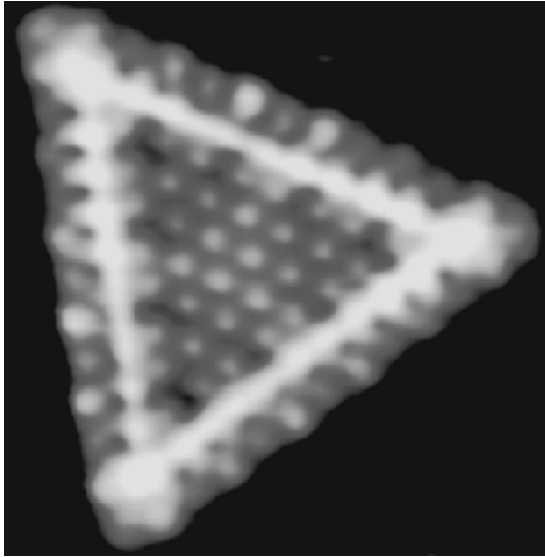The triangular shape implies that all three sides will be terminated by the same type of edge, i.e., either an Mo edge

FIG. 19. An STM image of a triangular MoS$_2$ nanocluster (48×53 Å^2, $U_t = 5.3$ mV, $I_t = 1.28$ nA). The cluster is synthesized with $p_{H_2S} = 10^{-9}$ bars and $T = 673$ K. (Figure adapted from Ref. 7.)

or an S edge. In Fig. 19 it is clearly seen that a bright brim of high conductance extends in the row behind the edges. As discussed in Sec. VI the nonzero current measured in the interior of the cluster is due to the Au substrate and we can associate the protrusions in this region with the triangular S atom lattice. However, in terms of this lattice the protrusions in the outermost row are seen to be shifted by half a lattice constant. The intensity of these protrusions also shows a variation with a periodicity of two lattice constants: every second protrusion is imaged more clearly than its two neighbors.

Comparing with Fig. 6(a) we see that the characteristic features observed for the MoS$_2$ triangle are also retained in the simulated image of an Mo edge with S dimers adsorbed. We are thus led to conclude that the observed edge structure can be associated with this configuration. There is, however, a difference between the two images. As described above, the experimental image displays a superstructure along the edges that is not retained in the simulated image of the infinite MoS$_2$ edge. This suggests that the observed superstructure is due to the finite length of the edges of the experimental structure. In fact, as discussed in Sec. X B recent DFT calculations on finite-size Mo edges display a similar periodicity due to a pairing of the S dimers.

In summary we have established that during the imaging of the MoS$_2$ triangles their sides are terminated by an Mo edge with S dimers adsorbed. In terms of the thermodynamic treatment this corresponds to situation (I) in Table II. Referring to Fig. 7 it can be seen that in the presence of the Au(111) substrate the S dimer configuration is indeed the most stable structure. In fact, the S dimers are expected to be stable even during sulfidation. We emphasize that a different result would be obtained if the effect of the substrate was

omitted. In that case the calculations for the isolated Mo edge show that the S monomer configuration is the more stable structure, cf. Fig. 4.

XII. SUMMARY

We have presented a detailed investigation of both the electronic and atomic structure of the edges of single-layer MoS$_2$. Depending on the edge termination several one-dimensional metallic edge states have been identified at both the Mo edge and the S edge. These intrinsic metallic states may be regarded as one-dimensional analogs to two-dimensional surface states. However, we have also identified a single edge configuration, the Mo edge with S monomers adsorbed, that is found to be semiconducting.

Using hydrogen as a probe the chemical activity of both the Mo edge and the S edge has been investigated. We find that the strongest hydrogen bonds are formed at the S edge thus suggesting this edge to be chemically more active than the Mo edge. However, a weak bond may also be formed between hydrogen and the Mo edge when S monomers are present.

In order to extend the DFT energies to finite temperatures a scheme for calculating the edge free energy in the presence of molecular H$_2$ and H$_2$S has been derived. We find that under HDS conditions hydrogen is expected to be adsorbed at both the Mo edge and the S edge in the form of S-H groups. The availability of activated hydrogen is an important prerequisite for the HDS process, and the results suggest that in order to understand the catalytic nature of the MoS$_2$ edges the presence of S-H groups must be taken into account. At the Mo edge it has been shown that both the insulating and the metallic edges may be stable. A metal-to-insulator transition can, for instance, be realized by suitably adjusting the partial pressures of H$_2$S and H$_2$.

The theoretical analysis has also been applied to a recent STM experiment on MoS$_2$ nanostructures. Simulated STM images have been compared with their experimental counterparts thereby providing an identification of the experimentally observed edge structures. It is found that the edges of the nanoclusters are associated with one-dimensional metallic edge states and the triangles can thus be regarded as closed, nanometer-sized wires. In general, we expect that these one-dimensional, metallic edge states will also pertain to other geometries, such as steps of the (0001) surface of bulk MoS$_2$. Having, for instance, an Mo edge with S dimers adsorbed, the step edge will be metallic having two localized, one-dimensional conducting channels. We suggest that such structures can be used as templates for future experimental studies of one-dimensional metallic systems on the nanometer length scale.[45]

[1] L. Margulls, G. Salltra, R. Tenne, and M. Tallanker, Nature (London) **365**, 113 (1993).

[2] H. Topsøe, B. S. Clausen, and F. E. Masooth, *Hydrotreating Catalysis* (Springer, Berlin, 1996).

[3] M. Chhowalla and G. A. J. Amaratunga, Nature (London) **407**, 164 (2000).

[4] L. Rapoport, Yu. Bilik, Y. Feldman, M. Homyonfer, S. R. Cohen, and R. Tenne, Nature (London) **387**, 791 (1997).

[5] M. V. Bollinger, J. V. Lauritsen, K. W. Jacobsen, J. K. Nørskov, S. Helveg, and F. Besenbacher, Phys. Rev. Lett. **87**, 196803 (2001).

[6] J. V. Barth, H. Brune, G. Ertl, and R. J. Behm, Phys. Rev. B **42**, 9307 (1990).

[7] S. Helveg, J. V. Lauritsen, E. Lægsgaard, I. Stensgaard, J. K. Nørskov, B. S. Clausen, H. Topsøe, and F. Besenbacher, Phys. Rev. Lett. **84**, 951 (2000).

[8] J. V. Lauritsen, S. Helveg, E. Lægsgaard, I. Stensgaard, B. S. Clausen, H. Topsøe, and F. Besenbacher, J. Catal. **197**, 1 (2001).

[9] B. Hammer and O. H. Nielsen, in *Workshop on Applied Parallel Computing in Physics, Chemistry, Engineering Science (PARA95)*, edited by J. Wasniewski, Vol. 1041 of *Springer Lecture Notes in Computer Science* (Springer, Berlin, 1995).

[10] B. Hammer, L. B. Hansen, and J. K. Nørskov, Phys. Rev. B **59**, 7413 (1999).

[11] G. Kresse and J. Furthmüller, Comput. Mater. Sci. **6**, 15 (1996).

[12] Dacapo pseudopotential code; http://www.fysik.dtu.dk/campos

[13] We note that for the calculations on MoS$_2$ stripes with an underlying Au substrate a cutoff energy of 20 Ry for the KS wave functions is used. The electron density is still expanded in plane waves up to 25 Ry (Ref. 46).

[14] H. J. Monkhorst and J. D. Pack, Phys. Rev. B **13**, 5188 (1976).

[15] D. Vanderbilt, Phys. Rev. B **41**, 7892 (1990).

[16] J. P. Perdew, J. A. Chevary, S. H. Vosko, K. A. Jackson, M. R. Pederson, D. J. Singh, and C. Fiolhais, Phys. Rev. B **46**, 6671 (1992).

[17] M. Methfessel and A. T. Paxton, Phys. Rev. B **40**, 3616 (1989).

[18] P. Raybaud, J. Hafner, G. Kresse, S. Kasztelan, and H. Toulhoat, J. Catal. **189**, 129 (2000).

[19] X.-G. Wang, A. Chaka, and M. Scheffler, Phys. Rev. Lett. **84**, 3650 (2000).

[20] K. Reuter and M. Scheffler, Phys. Rev. B **65**, 035406 (2002).

[21] In this paper E will refer to a DFT energy unless otherwise explicitly specified.

[22] G. L. Frey, R. Tenne, M. J. Matthews, M. S. Dresselhaus, and G. Dresselhaus, Phys. Rev. B **60**, 2883 (1999).

[23] *CRC Handbook of Chemistry and Physics*, 64th ed., edited by R. C. Weast (Chemical Rubber, Cleveland, 1983).

[24] *NIST Chemistry WebBook: NIST Standard Reference Database Number 69*; http://webbook.nist.gov/chemistry/

[25] J. Tersoff and D. R. Hamann, Phys. Rev. Lett. **50**, 1998 (1983).

[26] J. Tersoff and D. R. Hamann, Phys. Rev. B **31**, 805 (1985).

[27] J. V. Lauritsen, S. Helveg, and F. Besenbacher (private communication).

[28] K. Kobayashi and J. Yamauchi, Phys. Rev. B **51**, 17 085 (1995).

[29] A. Altibelli, C. Joachim, and P. Sautet, Surf. Sci. **367**, 209 (1996).

[30] Th. Böker, R. Severin, C. Janowitz, R. Manzke, D. Voß, P. Krüger, A. Mazur, and J. Pollmann, Phys. Rev. B **64**, 235305 (2001).

[31] E. Hult, H. Rydberg, B. I. Lundqvist, and D. C. Langreth, Phys. Rev. B **59**, 4708 (1999).

[32] R. O. Jones and O. Gunnarson, Rev. Mod. Phys. **61**, 689 (1989).

[33] B. Hammer and J. K. Nørskov, Nature (London) **376**, 238 (1995).

[34] L. S. Byskov, J. K. Nørskov, B. S. Clausen, and H. Topsøe, J. Catal. **187**, 109 (1999).

[35] H. Schweiger, P. Raybaud, G. Kresse, and H. Toulhoat, J. Catalysis **207**, 76 (2002).

[36] J. C. Slater and G. F. Koster, Phys. Rev. **94**, 1498 (1954).

[37] A. Zangwill, *Physics at Surfaces* (Cambridge University, Cambridge, England, 1988).

[38] M. V. Bollinger, J. V. Lauritsen, K. W. Jacobsen, J. K. Nørskov, and F. Besenbacher (unpublished).

[39] M. Salmeron, G. A. Somorjai, A. Wold, R. Chianelli, and K. S. Liang, Chem. Phys. Lett. **90**, 105 (1982).

[40] L. S. Byskov, M. Bollinger, J. K. Nørskov, B. S. Clausen, and H. Topsøe, J. Mol. Catal. A: Chem. **163**, 117 (2000).

[41] S. Cristol, J. F. Paul, E. Payen, D. Bougeard, S. Clémondot, and F. Hutschka, J. Phys. Chem. B **106**, 5659 (2002).

[42] A. Travert, H. Nakamura, R. A. van Santen, S. Cristol, J.-F. Paul, and E. Payen, J. Am. Chem. Soc. **124**, 7084 (2002).

[43] J. V. Lauritsen, M. Nyberg, R. T. Vang, M. V. Bollinger, B. S. Clausen, H. Topsøe, K. W. Jacobsen, J. K. Nørskov, E. Lægsgaard, and F. Besenbacher (unpublished).

[44] Additional calculational details for the MoS$_2$ triangles: The double grid technique (Ref. 46) is applied where the wave functions consist of plane waves with a maximum kinetic energy of 18 Ry whereas the plane waves of the electron density, as before, have energies up to 25 Ry. The Brillouin-zone integration is performed with the Γ point only.

[45] F. J. Himpsel, K. N. Altmann, R. Bennewitz, J. N. Crain, A. Kirakosian, J.-L. Lin, and J. L. McChesney, J. Phys.: Condens. Matter **13**, 11 097 (2001).

[46] K. Laasonen, A. Pasquarello, R. Car, C. Lee, and D. Vanderbilt, Phys. Rev. B **47**, 10 142 (1993).